PCCP

Accepted Manuscript

ROYAL SOCIETY OF CHEMISTRY

www.rsc.org/pccp

Journal Name

ARTICLE TYPE

Cite this: DOI: 10.1039/xxxxxxxxxx

Density functional investigation and some optical experiments on dye-sensitized quantum dots†

Kalpna Jain,[a] Sreejith Kaniyankandy,[b] Shyam Kishor,[c] Ida Josefsson,[d] Hirendra N. Ghosh,[b] Khundrakpam S. Singh,[a] Sumit Mookerjee,[e] Michael Odelius,[d] and Lavanya M. Ramaniah,*[f]

Received Date
Accepted Date

DOI: 10.1039/xxxxxxxxxx

www.rsc.org/journalname

Dye-sensitized quantum dots (QDs) are promising candidates for dye-sensitized solar cells (DSSC). Here, we report steady state (absorption and photoluminescence) optical measurements on several sizes of CdS QDs ligated with Coumarin 343 dye (C-343) and two different solvents, viz., chloroform and toluene. We further report detailed first principles density functional theory and time-dependent density functional theory studies of the geometric, electronic and optical (absorption and emission) properties of three different sized capped QDs, ligated with C-343 dye. The absorption spectrum shows a QD-size-independent peak, and another peak which shifts to the blue with decrease in QD size. The first peak is found to arise from the dye molecule and the second one from the QD. Charge transfer using natural transition orbitals (NTOs) is found to occur from dye-to-QD and is solvent-dependent. In the emission spectra, the luminescence intensity of the dye is quenched by the addition of the QD indicating a strong interaction between the QD and the dye.

Keywords: DFT, quantum confinement, charge transfer, TDDFT, solar cell.

1 Introduction

Dye-sensitized solar cells (DSSC), designed by Grätzel and coworkers [1] in the 1990s, have revolutionized the field of cost effective photovoltaics (PV) with efficiencies close to 11 % [2,3]. The DSSC uses a combination of a sensitizer (light harvester) coated in a monolayer onto a nano-crystalline semiconductor with low photoactivity in the optical spectrum. The latter is directly supported by a transparent electrode on one side, while the sensitizer is connected to the back electrode via a liquid electrolyte or a solid hole conducting material. The sensitizer absorbs solar energy photons, each of which creates an electron hole pair, which should be separated as rapidly as possible to avoid losses through recombination. The initial step of the photovoltaic process is a light induced electron injection from the sensitizer into the semiconductor. While the holes are carried through an electrolyte to the counter-electrode, the electrons pass through another electrode and an external load, finally reaching the counter-electrode. The earliest DSSCs utilized nanocrystalline TiO_2, which is a bulk semiconductor, and a metalloorganic dye as the sensitizer.

The highest-performance DSSC devices based on liquid electrolytes use Ru(II)-based dyes [4–6], although a number of metal-free dyes [7,8] are very promising. To improve the absorption in the near infrared region some new approaches have been reported [4,9–11], such as the use of a combination of sensitizers with complementary absorption in the red and near-infra-red regions [9–11]. An alternative approach is to use the near-infrared dye as an energy relay dye to produce additional photocurrent [4].

Recently, solar cells using semiconductor quantum dots (QDs) have also elicited much interest due to the remarkable tunability of their optical and electronic properties in the size-quantized regime, which offer significant advantages, as different regions of the solar spectrum may be tapped. This has been shown in studies [12–14] with QDs as sensitizers for wide band gap semiconductors such as TiO_2, ZnO, and SnO_2 etc.. Novel properties of QDs such as multiple exciton generation may also help break the Shockley-Quiesser thermodynamic efficiency limit, which is ≈ 33 % for a single junction PV-cell [15].

However, efficiencies of QD-sensitized solar cells are only ≈

[a] Department of Physics, D. J. College, Baraut, Uttar Pradesh 250611, India.
[b] Chemistry Division, Bhabha Atomic Research Centre, Trombay, Mumbai 400085, India.
[c] Department of Chemistry, J. V. College, Baraut, Uttar Pradesh 250611, India.
[d] Department of Physics, Stockholm University, AlbaNova University Center, 106 91 Stockholm, Sweden.
[e] Inter University Accelerator Centre, Aruna Asaf Ali Marg, New Delhi 110067, India.
[f] High Pressure and Synchrotron Radiation Physics Divison, Physics Group, Bhabha Atomic Research Centre, Trombay, Mumbai 400085, India.

† Electronic Supplementary Information (ESI) available: [Tables showing the atomic contribution to frontier molecular orbitals, optical data for theoretical absorption spectra with diffuse basis sets and additional plots illustrating molecular orbitals, energy levels and optical absorption spectra.]. See DOI: 10.1039/b000000x/

5 %[16]. The low efficiencies are due to the rapid carrier recombination processes in these materials. To slow down electron-hole recombination, various structural modifications can be introduced to increase the electron or hole transfer rate from the QD-sensitizer[17].

One such modification is based on dye-QD co-sensitized systems.[18–23]. For instance, the fast photo-induced hole transfer from CdSe QD to the ruthenium dyes prevents electron-hole recombination between the transferred electron at the TiO2 surface and the trapped hole in the QD[17–19]. A similiar approach has been used for CdS QDs using N3 dye and a ZnS layer to prevent recombination[23]. Another case in which both QD and dye are used as bilayer sensitizers[20] for TiO_2 has given a 250 % increase in cell efficiency compared to a QD monolayer cell. Thus, dye-QD adducts can simultaneously serve many requirements[18] for light harvesting materials such as extension of the spectral absorption range by adding up the absorption ranges of both dye and QD[20], reduction of the recombination losses[19,21,23] and improvement of charge extraction[22].

In most studies, QDs are used as the light harvesting species. However, one can imagine a QD in the role of an acceptor, similar to the role of TiO_2, SnO_2 etc. as wide band gap semiconductors. Recent studies[2,3] report one such configuration, with a thin film of ZnO QDs, though the efficiency (7.5 %)[24] is less than that of TiO_2. However, there are very few detailed studies[25] on PVs with different sized QDs used in place of wide band gap semiconductors, with the dye harvesting visible light; in other words, dye-sensitized QDs. Such a configuration has several advantages for the design of PVs, such as : the band alignment may be modulated by varying the size, which in turn affects the open-circuit voltage (V_{oc}); the charger transfer rates may be modulated as the density of states (DOS) decreases with size; the influence of the solvent on charge carrier dynamics can be investigated since QDs are dispersible in many solvent media.

Larger efficiencies might have been achieved by tailoring the size of TiO_2 in TiO_2 based DSSC, provided the band edge position varies with size. However, for TiO_2, such size quantisation is seen only in the ultra small size regime at sizes <2 nm, due to the large effective mass of the electrons $\approx 10m_e$. In fact, to this day, such a large shift in absorption spectra has not been reported in the literature.

An understanding of the basic science aspects including the electronic structure, surface states, generation and recombination of charge carriers, etc. is important to fine-tune PV parameters. QDs have a significant fraction of atoms on the surface. These surface atoms have a coordination different from that of bulk atoms, leading to the possible creation of trap states on the surface falling in the energy band gap, and causing non-radiative relaxation of carriers, thereby adversely affecting PV efficiency. Hence, it is important to eliminate dangling bonds in these systems[26,27]. This can be achieved by surface passivation by attaching ligands to the QD surface and allowing for surface reconstruction. Interestingly, PbS/CdS core-shell QDs have also led to enhanced efficiencies as the wide-band gap CdS leads to passivation of the trap states[13]. Thus, further rigorous studies of surface passivation are required to design systems with optimal optoelectronic properties.

Various experiments have used dyes as functional groups for CdSe[19,28–31], PbS[32,33], and ZnO[25] QDs to facilitate charge transfer processes[17]. For instance, photoinduced charge transfer between QDs and Ru-polypyridine complexes has been shown for CdSe QDs[28] and ultrafast charge separation and recombination dynamics has been shown for lead sulphide QDs with methylene blue complexes probed by electron and hole intraband transitions[32]. When modified N719 dyes were used as sensitizers for ZnO QD-based flexible solar cells, the PV properties were enhanced significantly[25]. We note that charge transfer from the dye to the QD (or vice versa), depends on the QD material, size, interaction with the QD surface etc.[17,28,31,34].

Theoretical studies, in particular, first principles density functional theory (DFT) studies, have also been carried out to study various complex processes in DSSCs and QDSCs[17,35–37]. For instance, the conditions for directional charge transfer in CdSe QDs[17] functionalized by Ru(II) polypyridine complexes have been explained with the help of the relative positions of their energy levels. Similar study has been carried out in QDSCs based on anatase TiO_2 nanotubes (NT)[35] in which adsorbate states are introduced in the band gap of the TiO_2 NT upon the adsorption of a CdS QD on the TiO_2 NT surface. Another approach using non-adiabatic molecular dynamics (NAMD) has been reported for DSSC[36] and QDSC[37]. Thus, charge relaxation and recombination in dye-sensitized TiO_2[36] have been studied, as has ultrafast electron injection from a PbSe QD into the TiO_2 surface[37]. Based on a time-dependent self-consistent density functional tight-binding (TD-DFTB) approach, a novel method to predict photoinjection mechanisms in dye-sensitized TiO_2 solar cells has been investigated[38]. TDDFT calculations of the optical properties of DSSCs with TiO2 nanoparticles sensitized with two coumarine dyes, NKX-2311 and NKX-2593, have been reported in the literature[39]. Similar approaches for modeling charge recombination in DSSCs have been shown using first-principles electron dynamics[40]. Other DFT studies[41–43] have also yielded insight into the nature of charge transfer in DSSCs.

However, despite these reports, there is a need for more detailed DFT studies on dye-sensitized QDs. Further detailed optical absorption and emission studies using TDDFT need to be carried out, as should studies on charge transfer be described with the help of TDDFT. Such theoretical studies could induce more precise experiments.

In this paper, we report detailed theoretical studies on different-sized dye-sensitized CdS QDs. These systems have also been studied by experimental absorption and emission techniques. First principles density functional theory (DFT) and timedependent density functional theory (TDDFT) studies have been carried out, to determine the structural, electronic and optical properties of three different-sized CdS QDs, with passivating ligands and dye molecules attached, and solvated in solvents used in the experiments. The direction and nature of charge transfer during both absorption and emission are shown with the help of natural transition orbitals in a detailed manner for the first time for these types of systems. The paper is organized as follows. Section 2 contains details of the experiments carried out in this investigation, followed in Section 3 by the theoretical and com-

putational methodologies employed. In Section 4, the results and discussions are presented and the conclusions are summarized in Section 5.

2 Methodology - Experimental Studies

2.1 Sample Preparation

A standard colloidal synthesis route, as reported elsewhere[2,3,44], with oleic acid as the capping agent, was used to synthesize CdS QDs of various sizes. The capping agent allows for solubility in several organic solvents, hence two different solvents, *viz.,* chloroform and toluene were used. The Coumarin 343 (C-343) dye was chosen as sensitizer. For the purpose of sensitization, 3.64×10^{-6} M of different sized QDs were dissolved. The concentrations were calculated from the extinction coefficient of different sized QDs[2,3,45]. The dye concentration was adjusted to an absorbance of 0.1 for all the samples. C-343 has an extinction coefficient of 44300 cm^{-1}/M at peak position $\approx$ 444 nm.[46]. Therefore, the concentration of C-343 is $\approx 2\mu$ M and the molar ratio of C-343 to QDs is $\approx$1. For the solvent-dependent study, the concentrations of the QD and the dye were chosen to be the same. The sensitization was carried out for 48 hours in the dark, as there is a possibility of photocatalysis if the dye holds the charge. The C-343 sensitized QD samples are labelled CdS-x. (where x=1-5 for different sized QD samples, in increasing order of size) respectively (Fig. 1). For the solvent-dependent study, CdS-4 samples were used for all solvents.

2.2 Steady State Optical Studies

The steady state photo physical properties were studied by optical absorption and photoluminescence spectroscopy for different sizes and in different solvents. These measurements were carried out using a diode laser-based spectrofluorimeter from IBH (U.K.), which works on the principle of time-correlated single-photon counting. 453 nm (2.73 eV) LED was used as the excitation light source and a TBX4 detection module (IBH) coupled with a special Hamamatsu PMT was used for fluorescence detection. The 453 nm excitation was chosen specifically to avoid exciting the red edges of the largest CdS sample. Furthermore, 453 nm excitation excites the dye close to the peak of the $S_0 - S_1$ transition.

3 Methodology - Theoretical and Computational Details

First principles calculations were carried out within the framework of density functional theory (DFT) using the B3LYP functional and the 6-311G(d,p)/LANL2DZ basis sets as implemented in the Gaussian 09 software package[47] using Intel(R) Xeon(R) CPU X5472@ 3.00GHz MPI clusters. The 6-311G(d,p) basis set was chosen to describe H, C, N and O atoms, and effective core potentials[48,49] with a double-ζ valence basis set (LANL2DZ) were used for the Cd and S atoms.

The QDs were constructed to have an internal structure and surface saturation as close as possible to those obtained in experiments. The initial geometries of the $Cd_{16}S_{16}$, $Cd_{31}S_{31}$ and $Cd_{40}S_{40}$ clusters were constructed by spherical cuts from the bulk crystal structure. The 1:1 Cd:S ratio was obtained by addition or removal of surface atoms with a low degree of bond saturation. Before attaching the organic ligands to passivate the dangling bonds on the surface of the QDs, 2-coordinated sulphur atoms on the surface were removed to obtain Cd-terminated QDs. In place of oleic acid (the passivating agent used in the experiment), acetate ions (CH3COO-), as representative of long chain fatty acids, were used as passivating agents on the surface of the QDs. The number of acetate molecules was determined by a charge neutrality condition[50] (N_{Cd} (+2) + N_S (-2) + N_{Ac} (-1) = 0). This leads to complete passivation of the QD surface for the smallest QD and for the largest QD, but not for the mid-sized QD. We note that the actual value of surface passivation in the experimental QD samples is not known, but is expected to be greater than $\approx$ 50 %[51].

The QDs $Cd_{16}S_{13}(CH_3COO)_6$ (henceforth termed QD1), $Cd_{31}S_{28}(CH3COO)_6$ (henceforth termed QD2) and $Cd_{40}S_{38}(CH3COO)_6(2H)$ (henceforth termed QD3) thus constructed were chosen as model systems for our study. In the case of $Cd_{40}S_{40}$, after removal of two 2-coordinated sulphur atoms on the surface, six equivalent positions are available for acetate attachment. For these six acetate ions to be accommodated, two additional hydrogens were attached to maintain charge neutrality. The reason for making QD3 in this manner was to make a structure similar to QD1 (with one additional layer). To minimize the dangling bonds with lesser ligands, hydrogens were used. A similar approach has been used in an earlier work[27]. The dye-sensitized QDs were prepared by replacing one of the acetate ions with a C-343 dye molecule. The geometry of each cluster, thus prepared, was optimized without symmetry constraints until the residual forces were less than 0.00045 a.u.. In order to confirm that the stationary point obtained corresponds to a local minimum, frequency calculations, which at a true minimum yield a Hessian with only positive eigenvalues, were performed at the same level of the theory. The electronic properties *viz.*, the projected density of states (PDOS), the highest occupied molecular orbital (HOMO) and the lowest unoccupied molecular orbital (LUMO), of the cluster were then determined[47,52,53].

The PDOS were computed using a double-zeta-valence-polarized (DZVP) basis set[52–54] to avoid problems with assignment of atomic charges in the Mulliken population analysis with the large basis set. The convolution of the PDOS was done using a gaussian function with a half-width of 0.5 eV. The open-circuit voltage, which is the maximum thermodynamically allowed voltage that can be obtained from a PV cell, was calculated as the difference between the lowest level of the CB of the QD and the HOMO level of the electron injector, *i.e.*, the dye. This estimated value of V_{oc} can be compared with the values obtained for other PV cells. In order to compute the absorption spectrum, time dependent density functional theory (TDDFT) calculations were carried out at the same level of accuracy as the DFT calculation mentioned above. The vertical excitation energies, excluding zero-point energies, and oscillator strengths were calculated at the ground state geometries. These calculations were repeated adding diffuse functions to the basis set 6-311++G(d,p) for the smallest dye-sensitized QD in vacuum and in both solvents.

The emission spectra were also calculated at the same level of

accuracy as that of absorption. For this, the TDDFT excited states with a large oscillator strength in the absorption spectrum are chosen, and the structure is geometry optimized in these states.

Natural transition orbitals (NTOs)[55] are used to understand the charge transfer within the system, upon absorption or emission. As discussed in Ref.[55], the NTO approach relies on finding a compact orbital representation for the electronic transition density matrix. Separate unitary transformations are applied to the occupied and the virtual orbitals so that there is a correspondence between the excited particle and the empty hole[55,56].

Solvent effects for both absorption and emission spectra were modelled using the polarizable continuum model (PCM)[57,58]. In the PCM, the solvent is modelled as a continuum, infinite, homogeneous and isotropic dielectric medium, characterized by a dielectric constant (ε). The molecule is placed in a cavity modelled on its shape, and the electrostatic solute-solvent interactions are calculated by introducing an apparent surface charge distribution spread on the cavity surface. The solvent effects were calculated for chloroform ($\varepsilon = 4.71$)and toluene ($\varepsilon = 2.37$) solvents in order to make contact with the experiments.

4 Results and discussion

4.1 Size determination of QDs

In our study CdS QDs of different sizes were employed as acceptors. As the exciton Bohr radius for CdS is ≈ 3 nm, size quantization effects would be important in these small QDs. Hence, the electron (or hole) energies in the QD would be shifted upwards (or downwards) from the bulk CB (or VB) edge (Fig. 1). While a qualitative picture of these shifts may be obtained from Effective Mass theory[59], a detailed understanding requires a more sophisticated theory, such as tight binding (TB) theory, which includes band non-parabolicity and band-mixing effects. Using TB theory, the size dependence of the electronic spectra, exciton peaks and absorption spectra of bare QDs for various sizes and materials have been studied earlier[60–62]. While DFT calculations could in principle also yield the quantum size effects accurately, these are presently far too expensive to carry out for all but the smallest QDs. The experimental optical absorption spectra of the cleaned QD samples (bare QDs with passivating agents attached) in this study are shown in Fig. 1. The experimental peaks are fitted to the theoretical TB curve for the exciton position as a function of size to determine the sizes of the various bare QDs. These sizes are given in Table 1.

4.2 Geometric Structure

The main structural features of the model systems obtained after geometry optimization using DFT are discussed in what follows. The optimized structures of the passivated QDs and dye-sensitized QDs are given in Fig. 2.

4.2.1 Passivated QDs

In all the three acetate passivated QDs, there are some common structural features observed after optimization, and these are briefly reported in Table 2. The optimization leads to surface reconstruction. In our case, only the mid-sized QD (QD2) had 2-coordinated Cd and S atoms on the surface of the unrelaxed structure. After surface reconstruction, all the 2-coordinated surface atoms became either 3-coordinated or 4-coordinated. The variations in bond length and bond angle are least for the smallest sized QD (QD1) and maximum for QD2. In the optimized structures, the surface Cd-S bonds are shorter than the bonds at the center of the clusters. In comparison to the 4-coordinated Cd-S bond lengths (2.88 Å) at the center of the largest cluster (QD3), the Cd-S bond length around the 3-coordinated Cd or S atoms are found to be in the range 2.47 Å- 2.82 Å. Hence, lower coordination leads to surface reconstruction resulting in a shortening of bond length. The S-Cd-S bond angles around the 3-coordinated Cd atoms range from 98.60 ° to 143.99 °, larger than around the 4-coordinated Cd atoms, ranging from 99.07 ° to 128.18 °. On the other hand, in the case of Cd-S-Cd, the bond angles around the 3-coordinated S atoms range from 92.96 ° to 111.52 °, and are smaller than those around the 4-coordinated S atoms 98.40 ° to 118.74 °. Interestingly, the variation around the 3-coordinated Cd and S atoms is least in the case of the smallest QD system(QD1). Also, in QD1 the angles around the 4-coordinated Cd and S atoms are very close to 109.47 °. For QD2, due to the maximum surface reconstruction, the bond angle variation around the surface Cd and S atoms is maximum. The bond angles around the 4-coordinated S atoms involving oxygen of acetate (Fig. 2(inset)) range from 68.92° to 149.74°.

In the three passivated QDs, there are three distinct sets of Cd-O bonds ($Cd_A - O_A$, $Cd_B - O_B$ and $Cd_B - O_A$) involving acetate groups. This is because the orientation of the acetate group in the optimized structures is found to be of the "tilted bridge" type[50] (Fig. 2(inset)), in which one O of the acetate group is coordinated to two surface Cd atoms, and the other O of the acetate group is coordinated to just one surface Cd atom. The shortest $Cd_A - O_A$ bond length ranges between 2.20 Å- 2.25 Åand the longest $Cd_B - O_A$ ranges between 2.28 Å- 2.33 Å. This is true even when the initial structure has a different configuration, such as one O attached to two Cd atoms with the other O non-bonded. This is suggestive of the formation of a strong bond between the carboxylate O and surface Cd. We note that the bond lengths are similar to (one set of) Cd-O bond lengths observed in Cd carboxylate salts such as cadmium diacetate dihydrate (2.30Å)[63]. The surface Cd atoms also assume the bulk tetrahedral structure, as the angle (φ) between the O-Cd-O plane and the S-Cd-S plane (Fig. 2(inset)) lies in the range 88.52 ° - 92.37 ° for QD1 and QD3. In variation is large in case of QD2 (68.92 ° - 149.74 °). The bond lengths of the two C-O bonds of acetates attached to the surface Cd differ in the optimized structures. The C-O bond length for the doubly-coordinated oxygen (O_A) is elongated ($\approx 1.28 \pm 0.01$Å) with respect to the singly-coordinated O_B (1.24Å).

We note that the QD1 may be said to be a fullerene analogue (Fig. 2), similar to the highly stable structure discussed in Ref.[64], which is made up solely of 4-membered and 6-membered rings of Cd and S atoms. Our QD1 studied here consists of only 6-membered rings, and these hexagonal rings forming the cage consist of Cd-S-Cd bonds as well as Cd-O-Cd bonds. It also has a S atom at the centre of the cage.

4.2.2 Dye-sensitized QDs

The dye-sensitized QDs were constructed by taking the optimized structure of the acetate - passivated QDs (QD1, QD2 or QD3), replacing one of the acetate molecules by a C-343 dye molecule, and optimizing the resulting dye-sensitized QD. These optimized structures for the dye-sensitized QDs are given in Fig. 2. In all of these, as also in the passivated QDs, the tilted bridge form (in which one of the oxygens bond to two Cd atoms)is found to be preferred over the bridge form (in which each O is coordinated to just one Cd). A vibrational analysis of the bridge structure in Fig. 2 gives an imaginary frequency, which implies that the structure is a transition (unstable) state. This state has an energy that is 0.13 eV higher than the optimised structure with tilted bridge geometry and is therefore not thermally accessible.

Finally, we note that in the optimized structures, the orientation of the carboxylate group of the dye is similar to the orientation of the acetate. The angle between the O-Cd-O plane containing the carboxylate and the S-Cd-S plane is 95.43°, 105.25° and 84.58° for dye-QD1, dye-QD2 and dye-QD3, respectively.

4.3 Electronic structure

The computed Kohn-Sham energies corresponding to the passivated QDs, free dye, and dye-sensitized QDs are given in Fig. 3.

4.3.1 Passivated QDs

The percentage contributions from various atoms to the energy levels for the passivated QDs are given in Table S1 of Supporting Information. The states corresponding to the near-VB-edge levels such as the HOMO, HOMO-1 and HOMO-2, and near-CB-edge levels such as the LUMO, are delocalized over the whole QD. While the former have contributions from both 3- and 4- coordinated S atoms, the latter have major contributions from the 3-coordinated Cd atoms. The levels due to the passivating agent (acetate) in the passivated QDs are not at the VB and CB edges. Similar observations have been reported in an earlier study on acetate - passivated CdSe QDs[50].

4.3.2 Dye-sensitized QDs

Figs. 3 and 4 show that the dye molecule on the QD introduces several levels deep in the VB and CB, as well as a single level in the energy band gap which becomes the HOMO. The relative positions of the HOMO and LUMO of dye and QD, *i.e.*, the band alignment, is found to be modulated by varying the size of the QD. The free C-343 HOMO is located within the passivated QD's HOMO - LUMO gap, while the LUMO is located above the LUMO of the QD and in the CB of the passivated QD. The molecular orbital (MO) plots (see Supporting Information, Fig. S1) show that for all the dye-sensitized QDs, the HOMO is spread only over the dye and the LUMO is spread only over the QD. On attachment of dye to passivated QD, the energy levels of dye and QD occur in the same energy range, with the possibility of mixing between the levels, resulting in good interaction between dye and QD. On solvating the dye-sensitized QD, HOMO arises from the dye but the LUMO has both dye and QD components (chloroform) and QD alone (toluene)(Fig. S2).

4.4 Steady State Absorption and Emission Spectra

Along with the results of our DFT calculations, we continue with the presentation of the results from the experimental measurements of optical spectra.

4.4.1 Absorption spectra

4.4.1.1 Test on C-343 dye In Fig. 5 we present a comparison between experiments and the calculated absorption spectrum (valence excitation transitions for the ground state geometry) of the dye, using TDDFT and neglecting zero point energy and final state dynamics. The calculations were carried out in the gas phase, as well as in solution using the PCM as mentioned earlier. The experimental and theoretical (our work and earlier calculations) optical data are summarized in Tables 3 (gas phase) and 4 (solution). While our theory is in good agreement with previous calculations[65,66], there is a discrepancy of $\approx$ 400 meV with the experimental absorption spectrum. This may be taken as the error bar for the DFT, TDDFT and PCM calculations[66,67], and is either due to problems in the description of the electronic excitations or due to crudeness of the implicit solvation PCM model.

4.4.1.2 Dye-sensitized QDs The experimental absorption spectra (Fig. 5) for the dye-sensitized QDs in chloroform solvent show (a) peaks in the range 3.0-3.5 eV and (b) a peak at 2.8 eV. The first set of peaks is also present in the absorption spectra of the cleaned QDs (Fig. 1) and thus arises from the QD. The peak at 2.8 eV does not change with the QD size, which implies that this arises from the dye molecule. This is consistent with the theoretical calculations for all the dye-sensitized QD systems, as the theoretical peak at $\approx$ 3.39 eV (in vacuum) does not change with the size (the shift of the order of 0.18 eV is within the error bars of our calculation).

The experimental difficulties with preparing a monodispersive distribution of QD small enough that it can be modelled faithfully in the calculations make a direct assessment of different aspects of the calculations difficult. However, we note that the employed model neglects a microscopic treatment of the solvent effects, and we also do not have detailed experimental information on the adsorption geometries of the capping agents. Also, more elaborate methods for modelling the electronic excitations could be investigated in future studies.

We note that in the experiments reported in this work, the QD size is such that the absorption in the dye-QD system does not overlap with that of the dye. However, in all the three dye-sensitized QDs studied theoretically, the QD size is such that, in each case, the absorption peak of the QD overlaps with that of the dye. (See Fig. 5). (We also note that, as expected, the theoretical peaks in the passivated QDs in vacuum are red-shifted as the QD size increases.) Hence, the theoretical absorption peak of the dye-sensitized QDs is almost double that of the isolated dye and passivated QDs. While this enhanced light absorption leading to additional carriers is a welcome feature, on the other hand, the light photons absorbed directly by the QD would not be useful due to enhanced recombination of the resulting electron-hole pair localized on the QD. We note that a similar additive spectral feature had been earlier reported for CdSe/Ru(II)bpy composites[17,68] and in fluorescein-sensitized QDs[69].

To understand these absorption spectra better, NTOs calculated for the excited states with large oscillator strengths have been plotted in Fig. 6. The last column of Tables III and IV report the largest NTO eigenvalue for each state. The eigenvalue is in the range 0.75-0.98 for all the states, signifying that the states can be quite well described in terms of a dominant excitation pair accounting for over 75-98% of the transition. In each panel, the hole charge density distribution in the ground state is indicated on the left, and the electron charge density distribution in the given excited state is indicated on the right. Except for a few cases (to be discussed later), only those transitions in each of which the oscillator strength is greater than 0.1 are considered (Fig. 6). For all the dye-QD systems, there are both dye-to-dye transitions and QD-to-QD transitions, which is consistent with the fact that the dye and QD absorption spectra overlap at some frequencies. The total absorption spectra for dye-QD in chloroform and toluene are different, as shown also by the NTO analysis (Fig. 6). Very interestingly, there are also dye-to-QD transitions (i.e., charge-transfer excitations) in most of the dye-QD systems. (Fig. 6(a) - Excited states 3, 6 and 9 for dye-QD1 in vacuum; Fig. 6(b) - Excited state 1 for dye-QD1 in chloroform; Fig. 6(d) - Excited state 42 for dye-QD1 in vacuum; Fig. 6(e) - Excited states 43 and 51 for dye-QD2 in vacuum). From Fig. 6(a)-(c), we see that the dye-to-QD transitions seem to be suppressed in the presence of the solvent. The degree of suppression is slight in chloroform and much more in toluene (in which there is no dye-to-QD transition). This indicates that the dye-QD interaction is reduced by the presence of the solvent, to a smaller extent by chloroform and more by toluene. This is justified by the energy level diagram (Fig. S2) where a mixing was observed in LUMO level in chloroform and not in toluene. This is borne out by the fact that in the dye-QD1 system, in vacuum and in chloroform solvent, the dye-to-dye transition is shifted (shift is $\approx$ 0.09 eV in vacuum; while in chloroform, the shift is less, $\approx$ 0.04 eV) from that in the free dye; but in toluene solvent, there is a strong dye-to-dye transition (Fig. 6(c), excited state 4) at almost the same frequency as in the free dye (3.199 eV, shift of 0.003 eV).

To the best of our knowledge, this is the first detailed theoretical study of charge-transfer excitations using NTOs in these systems. This theoretical insight assumes greater significance in view of the fact that the experiments do not shed light on the question of the occurrence of charge-transfer excitations in these systems.

4.4.1.3 Solvent Effects The experimental solvent phase absorption spectra for C-343 dye in chloroform and toluene are given in Fig. 5. The absorption spectra vary in different solvents, which is also seen in the theoretical spectra calculated using the PCM[57,58] (Fig. 5 and Table 4), and may be attributed to the difference in polarities of the solvents (the dielectric constants of chloroform and toluene are 4.7113 and 2.3741, respectively). For the dye-QD1 system in chloroform, the strongest transition is from dye-to-dye while in toluene the dye-to-dye and QD-to-QD transitions are comparable in strength. As mentioned earlier, in the dye-QD1 system, the presence of the solvent seems to suppress charge-transfer from dye to QD. In the case of dye-QD1, in both the solvent, a red shift($\approx$ 120 meV) has been observed, and there is an additional hypsosochromic effect (increase in intensity by $\approx$ 30%). It should be mentioned that the PCM may be of limited applicability in solvents for which non-electrostatic effects are important[70].

4.4.1.4 Effect of diffuse function To see the effect of the diffuse function the calculations were repeated adding a diffuse function to the basis set (6-311++G(d,p)) for the smallest dye sensitized QD in vacuum and both solvents. The absorption spectra, NTO and the optical data are reported in Supporting Information Figs. S3, S4 and Table S2 respectively. We observe a marginal red-shift of $\approx$ 0.03 eV.

4.4.2 Emission spectra

4.4.2.1 Test on C-343 Dye The experimental photoluminescence spectrum of C-343 dye is shown in Fig. 7. The corresponding calculated emission spectrum is also shown in the same figure. To calculate the emission spectrum, we have to consider separately relaxation in each excited state and the subsequent decay to each of these relaxated states. To achieve a manageable calculation, we have restricted the number of excited states considered, such that the system was optimized only in those excited states for which the oscillator strength for the ground state absorption is larger than 0.1. In the C-343 dye in chloroform and toluene solvent, the first singlet excited state (S1) is the only state with significant oscillator strength in the absorption (Table 4). The theoretical and experimental emission peak values are given in Table 5. As in the case of the absorption spectra, our theoretical values are in good agreement with experimental values, with a discrepancy, ranging $\approx$ 400 meV, with the experiment, which is within the error bar of our calculations[66,67].

4.4.2.2 Dye-sensitized QDs The experimental emission spectra for dye-sensitized QDs clearly show a quench in luminescence intensity as compared to C-343 dye (Fig. 7). The calculated emission spectrum for the dye-QD1 in solution is shown for comparison. The absorption process gives different excited states, some with high oscillator strength. The system is separately optimized in each such state. We note that the theoretical emission spectrum comprises only the radiative process occurring between the chosen excited states and the ground state. Geometry optimization on an excited state potential energy surface is significantly more difficult than on the ground state potential energy surface, because in the majority of cases, there are several excited electronic states close in energy and it is difficult to distinguish between them and follow the desired one. In our system also, in a few select cases it became impossible to track the desired state due to frequent hopping in ground state orbitals. But, in the majority of cases, the ground state potential energy surface does not have other electronic state close in energy and it was easy to follow the desired ground state without hopping onto the surface of another electronic state. The theoretical emission spectra (Fig. 7) and the detailed description given in Table 5 also show a quench in luminescence intensity for dye-QD1. This indicates a strong interaction between the QD and the dye. This is also favorable for solar cell applications as the recombination rate has gone

down. We also note that our calculation, as well as our experiment gives a larger quench for the luminescence in chloroform than in toluene. The NTOs (Fig. 8) also show a large oscillator strength for the emission from dye-to-dye for the dye-QD systems in both chloroform and toluene. Though the experimentally observed quenching of the luminescence could in principle be due to processes of energy or charge transfer, here, energy transfer is not feasible due to the lack of overlap between absorption by the CdS QDs and emission by the C-343 dye. Therefore charge transfer is likely the only possibility. Band alignment and energetics dictates the charge-transfer process, and electron transfer is the preferred route for charge-transfer, which arises due to the free energy difference arising out of the band offset with respect to dye energy levels.

4.5 Solar cell performance

The open-circuit voltage, V_{oc} has been computed theoretically using band alignment and energetics, as the energy difference between the LUMO of the QD and the HOMO of the dye. Our calculated V_{oc} is in the range 2.3 - 2.9 V (Table 6). To obtain an idea of the V_{oc} values generally obtained, we note that the V_{oc} for the thin film solar cells such as dye-sensitized solar cells[71–73] are 0.664-0.716 V (experiment)[73], 0.462-0.758 V (experiment)[71], 0.553-0.730 V (experiment)[72] and 1.135-1.365 V (theory)[72]; quantum dot sensitized solar cells[13,14] are ≈ 0.44-0.59V (experiment)[13], 0.4-0.8 V (experiment)[14]; conjugated polymer based solar cells[74] are ≈ 0.4-1.0 V (experiment)[74] and 0.8-1.4 V (theory)[74]; and perovskite based solar cells are 0.68-0.88V (experiment)[75]. The experimental values are generally less than 1 V. Thus, the experimental values of V_{oc} are ≈ less than half the theoretical V_{oc}[72,74] (in the cases where they have been calculated) or the experimental energy gap between the absorber and the acceptor[71,72,76]. This discrepancy is due to factors such as mismatch between energy levels, recombination losses, measuring method limitations and others.

5 Conclusions

In this paper, an exhaustive theoretical study of a novel configuration for solar cells, based on dye-sensitized quantum dots (QDs), is presented. Steady state experiments determining photophysical properties (optical absorption and emis sion) have also been performed on five different sizes of oleic acid capped and coumarine (C-343) dye-sensitized CdS QDs. Detailed first-principles density functional theory (DFT) calculations of the structure and electronic properties, and time dependent density functional theory (TDDFT) calculations of the optical properties (both absorption and emission),have been carried out on model acetate-passivated QDs of three different sizes, sensitized with C-343 dye. The calculations were carried out for both, the system in the gas phase, as well as in chloroform and toluene solvents modeled by a polarizable continuum model.The structural calculations of the bond lengths and bond angles determined by geometry optimization indicate strong interaction of the passivating agent and sensitizer, with the QDs. The electronic structure study indicates that for all the dye-sensitized QDs, the HOMO is localized on the dye and the LUMO on the QD, a feature which is expected to facilitate electron transfer from dye to QD. The experimental absorption spectra for all the dye-QD systems studied show a size-independent peak at 2.76 eV attributable to the dye, and a peak which shifts to the blue with the decrease in QD size, which is attributable to the QD. These two peaks are well separated for all the QD sizes studied. The theoretical optical absorption spectra on the other hand show an overlap between the peak arising from the QD and the dye, for all the dye-QD systems studied. The theoretical dye peak occurs at 3.39 eV, in reasonable agreement with the experiment. The overall absorption spectra indicate a red shift of ≈ 0.2 eV in the solvent, as well as some small differences between the two solvents studied, chloroform and toluene, arising from the difference in their dielectric constants.

The theoretical absorption spectra are analyzed using Natural Transition Orbitals (NTO) for the first time in these systems. These indicate dye-to-dye, QD-to-QD and also interestingly, in some cases, dye-to-QD transitions. Our theoretical study thus provides information that is not accessible from the experiments, viz., the occurrence of charge-transfer excitations in the dye-QD systems. The presence of the solvent suppresses the dye-to-QD transition, and also lessens the shift of the dye-to-dye transition from the free dye value, indicating that the dye-QD interaction is lessened by the solvent. Chloroform solvent is found to better preserve dye-QD interaction than toluene solvent.

The calculated emission spectra are qualitatively similar to the experimental emission spectra, as the dye luminescence is found to be quenched (more in chloroform than in toluene) on attaching the QD, both in the experiment and in the TDDFT study. The theoretical open circuit voltage is found to be in the range 2.3 - 2.9 V. To conclude, dye-sensitized QDs offer an efficient PV configuration for solar cell applications.

Acknowledgements

This work was supported by a DAE-BRNS grant (Sanction No. 2010/37C/58/BRNS) and was possible due to the HPC facility and help from the staff of IUAC-New Delhi. MO acknowledges support from Stockholm University for an internationalization grant, the Swedish Research Council, Carl Tryggers Foundation, Magnus Bergvall Foundation. KJ thanks CSIR, New Delhi for a Junior Research Fellowship (JRF).

References

1 B. O'Regan, and M. Grätzel, *Nature*, 1991, **353**, 737.
2 J. A. Anta, E. Guillén, and R. Tena-Zaera, *J. Phys. Chem. C*, 2012, **116**, 11413.
3 Q. Zhang, C. S. Dandeneau, X. Zhou, and G. Cao, *Adv. Mater.*, 2009, **21**, 4087.
4 M. Pastore and F. De Angelis, *J. Phys. Chem. Lett.*, 2012, **3**, 2146.
5 M. K. Nazeeruddin, F. De Angelis, S. Fantacci, A. Selloni, G. Viscardi, P. Liska, S. Ito, B. Takeru and M. Grätzel, *J. Am. Chem. Soc.*, 2005, **127**, 16835.
6 M. Grätzel, *J. Photochem. Photobiol. A*, 2004, **164**, 3.

7 Y. Bai, J. Zhang, D. Zhou, Y. Wang, M. Zhang and P. Wang, *J. Am. Chem. Soc.* 2011, **133**, 11442.

8 M. Zhang, J. Liu, Y. Wang, D. Zhou and P. Wang, *Chem. Sci.*, 2011, **2**, 1401.

9 J. N. Clifford, A. Forneli, H. Chen, T. Torres, S. Tan and E. Palomares, *J. Mater. Chem.*, 2011, **21**, 1693.

10 K. Sayama, S. Tsukagoshi, T. Mori, K. Hara, Y. Ohga, A. Shinpou, Y. Abe, S. Suga and H. Arakawa, *Sol. Energy Mater. Sol. Cells*, 2003, **80**, 47.

11 M. V. Martínez-Díaz, de la Torre and T. Torres, *Chem. Commun.*, 2010, **46**, 7090.

12 G. Hodes, *J. Phys. Chem. C*, 2008, **112**, 17778.

13 M. J. Speirs, D. M. Balazs, H.-H. Fang, L.-H. Lai, L. Protesescu, M. V. Kovalenko, and M. A. Loi, *J. Mater. Chem. A, 2015, **3**, 1450*.

14 *M. G. Panthani, C. J. Stolle, D. K. Reid, D. J. Rhee, T. B. Harvey, V. A. Akhavan, Y. Yu, and B. A. Korgel, J. Phys. Chem. Lett.*, 2013, **4**, 2030.

15 R. Schaller, and V. Klimov, *Phys. Rev. Lett.*, 2004, **92**, 186601.

16 J.-W. Lee, D.-Y. Son, T. K. Ahn, H.-W. Shin, I. Y. Kim, S.-J. Hwang, M. J. Ko, S. Sul, H. Han and N.-G. Park, *Science Rep.*, 2013, **3**, 1050.

17 S. Kilina, P. Cui, S. A. Fischer, and S. Tretiak, *J. Phys. Chem. Lett.*, 2014, **5**, 3565.

18 S. Gimenez, A. L. Rogach, A. A. Lutich, D. Gross, A. Poeschl, A. S. Susha, I. Mora-Sero, T. Lana-Villarreal and J. Bisquert, *J. Appl. Phys.*, 2011, **110**, 014314.

19 I. Mora-Sero, V. Likodimos, S. Gimenez, E. Martinez-Ferrero, J. Albero, E. Palomares, A. G. Kontos, P. Falaras and J. Bisquert, *J. Phys. Chem. C*, 2010, **114**, 6755.

20 M. Shalom, J. Albero, Z. Tachan, E. Martínez-Ferrero, A. Zaban and E. Palomares *J. Phys. Chem. Lett.*, 2010, **1**, 1134.

21 I. Mora-Sero, T. Dittrich, A. S. Susha, A. L. Rogach, and J. Bisquert, *Thin Solid Films*, 2010, **516**, 6994.

22 H. C. Leventis and S. A. Haque, *Environ. Sci.*, 2009, **2**, 1176-1179.

23 H. Shen, J. Li, L. Zhao, S. Zhang, W. Wang, D. Oronf and H. Lin *Phys. Chem. Chem. Phys.*, 2014, **16**, 6250.

24 N. Memarian, I. Concina, A. Braga, S. M. Rozati, A. Vomiero, and G. Sberveglieri, *Angew. Chem., Int. Ed.*, 2011, **50**, 12321.

25 A. Pang, C. Chen, L. Chen, W. Liu and M. Wei, *RSC Adv.*, 2012, **2**, 9565.

26 S. Kilina, I. Sergei, and T. Sergei, *J. Am. Chem. Soc.*, 2009, **131**, 7717.

27 M. D. Ben, R. W. A. Havenith, R. Broer, and M. Stener, *J. Phys. Chem. C*, 2011, **115**, 16782.

28 M. Sykora, M. A. Petruska, J. Alstrum-Acevedo, I. Bezel, T. J. Meyer and V. I. Klimov, *J. Am. Chem. Soc.*, 2006, **128**, 9984.

29 J. Huang, D. Stockwell, Z. Huang, D. L. Mohler and T. Lian, *J. Am. Chem. Soc.*, 2008, **130**, 5632.

30 A. Boulesbaa, Z. Huang, D. Wu, T. Lian, *J. Phys. Chem. C*, 2010, **114**, 962.

31 A. J. Morris-Cohen, K. O. Aruda, A. M. Rasmussen, G. Canzi, T. Seideman, C. P. Kubiakb, E. A. Weiss, *Phys. Chem. Chem. Phys.*, 2012, **14**, 13794.

32 Y. Yang, W. Rodriguez-Cordoba and T. Lian, *J. Am. Chem. Soc.*, 2011, **133**, 9246.

33 K. E. Knowles, M. Malicki, R. Parameswaran, L. C. Cass and E. A. Weiss, *J. Am. Chem. Soc.*, 2013, **135**, 7264.

34 E. A. McArthur, J. M. Godbe, D. B. Tice and E. A. Weiss, *J. Phys. Chem. C*, 2012, **116**, 6136.

35 C. Dong, X. Li, and J. Qi, *J. Phys. Chem. C*, 2011, **115**, 20307.

36 W. R. Duncan, C. F. Craig and O. V. Prezhdo, *J. Am. Chem. Soc.*, 2007, **129**, 8528.

37 R. Long and O. V. Prezhdo, *J. Am. Chem. Soc.*, 2011, **133**, 19240.

38 M. B. Oviedo, X. Zarate, C. F. A. Negre, E. Schott, R. Arratia-Pérez, and C. G. Sánchez, *J. Phys. Chem. Lett.*, 2012, **3**, 2548.

39 S. Agrawal, P. Dev, N. J. English, K. R. Thampi and J. M. D. MacElroy, *J. Mater. Chem.*, 2011, **21**, 11101.

40 W. Ma, Y. Jiao and S. Meng, *Phys. Chem. Chem. Phys.*, 2013, **15**, 17187.

41 S. K. Muzakir, N. Alias, M. M. Yusoffab and R. Jose, *Phys. Chem. Chem. Phys.*, 2013, **15**, 16275.

42 K. R. Siefermann et. al. *J. Phys. Chem. Lett.*, 2014, **5**, 2753.

43 M. M. Hedrick, M. L. Mayo, E. Badaeva and Svetlana Kilina, *J. Phys. Chem. C*, 2013, **117**, 18216.

44 R. B. Vasiliev, S. G. Dorofeev, D. N. Dirin, D. A. Belov, and T. A. Kuznetsova, *Mendeleev Commun.*, 2004, **14**, 169.

45 W. W. Yu, L. Qu, W. Guo, and X. Peng, *Chem. Mater.*, 2003, **15**, 2854.

46 G. A. Reynolds, and K. H. Drexhage, *Optics Commun.*, 1975, **13**, 222.

47 G. A. Frisch, et al. Gaussian 09, Revision C.01, Gaussian, Inc., 2010, Wallingford CT.

48 P. J. Hay, and W. R. Wadt, *J. Chem. Phys.*, 1985, **82**, 270.

49 P. J. Hay, and W. R. Wadt, *J. Chem. Phys.*, 1985, **82**, 299.

50 O. Voznyy, *J. Phys. Chem. C*, 2011, **115**, 15927.

51 O. V. Vassiltsova, Z. Zhao, M. A. Petrukhina, and M. A. Carpenter, *Sensor. Actuat. B-Chem.*, 2007, **123**, 522.

52 S. I. Gorelsky, AOMix: Program for Molecular Orbital Analysis, http://www.sg-chem.net/, 2013, version 6.80.

53 S. I. Gorelsky, and A. B. P. Lever, *J. Organomet. Chem.*, 2001, **635**, 187.

54 N. Godbout, D. R. Salahub, J. Andzelm, and E. Wimmer, *Can. J. Chem.*, 1992, **70**, 560.

55 Martin, and L. Richard, *J. Chem. Phys.*, 2003, **118**, 4775.

56 A. T. Amos, G. G. Hall, *Proc. R. Soc. Lond. A*, 1961, **263**, 483.

57 G. Scalmani, and M. J. Frisch, *J. Chem. Phys.*, 2010, **132**, 114110.

58 B. Mennucci, *WIREs Comput. Mol. Sci.*, 2012, **2**, 386.

59 L. E. Brus, *J. Chem. Phys.*, 1984, **80**, 4403.

60 L. M. Ramaniah, S. V. Nair, *Phys. Rev. B*, 1993, **47**, 7132.

61 S. V. Nair, L. M. Ramaniah, and K. C. Rustagi, *Phys. Rev. B*, 1992, **45**, 5969.

62 S. S. Dhayal, L. M. Ramaniah, H. E. Ruda, and S. V. Nair, *J. Chem. Phys.*, 2014, **141**, 204702.

63 W. Harrison, and J. Trotter, *J. Chem. Soc., Dalton Trans.*, 1972, 956.

64 A. Kasuya, R. Sivamohan, Y. A. Barnakov, I. M. Dmitruk, T. Nirasawa, V. R. Romanyuk, V. Kumar, S. V. Mamykin, K. Tohji, B. Jeyadevan, K. Shinoda, T. Kudo, O. Terasaki, Z. Liu, R. V. Belosludov, V. Sundararajan, and Y. Kawazoe, *Nature Mater.*, 2004, **3**, 99.

65 R. Sánchez-de-Armas, M. Á. S. Miguel, J. Oviedo, and J. F. Sanz, *Phys. Chem. Chem. Phys.*, 2012, **14**, 225.

66 Y. Kurashige, T. Nakajima, S. Kurashige, and K. Hirao, *J. Phys. Chem. A*, 2007, **111**, 5544.

67 S. Hazebroucq, F. Labat, D. Lincot, and C. Adamo, *J. Phys. Chem. A*, 2008, **112**, 7264.

68 M. Sykora, M. A. Petruska, J. Alstrum-Acevedo, I. Bezel, T. J. Meyer, and V. I. Klimov, *J. Am. Chem. Soc.*, 2006, **128**, 9984.

69 O. Carion, B. Mahler, T. Pons, and B. Dubertret, *Nature Protocols*, 2007, **2**, 2383.

70 B. Mennucci, J. Tomasi, R. Cammi, J. R. Cheeseman, M. J. Frisch, F. J. Devlin, F. Gabriel, and P. J. Stephens, *J. Phys. Chem. A*, 2002, **106**, 6102.

71 S. R. Raga, E. M. Barea, and F. Fabregat-Santiago, *J. Phys. Chem. Lett.*, 2012, **3**, 1629.

72 W. Ma, Y. Jiao, and S. Meng, *J. Phys. Chem. C*, 2014, **118**, 16447.

73 M. Cheng, X. Yang, C. Chen, J. Zhao, Q. Tana and L. Sun, *Phys. Chem. Chem. Phys.*, 2013, **15**, 17452.

74 N. Bérubé, V. Gosselin, J. Gaudreau, and M. Côté, *J. Phys. Chem. C*, 2013, **117**, 7964.

75 F. Hao, C. C. Stoumpos, D. H. Cao, R. P. H. Chang, and M. G. Kanatzidis, *Nature Photon*, 2014, **8**, 489.

76 M. C. Scharber, D. Mühlbacher, M. Koppe, P. Denk, C. Waldauf, A. J. Heeger, and C. J. Brabec, *Adv. Mater.*, 2006, **18**, 789.

77 K. Hara, T. Sato, R. Katoh, A. Furube, Y. Ohga, A. Shinpo, S. Suga, K. Sayama, H. Sugihara, and H. Arakawa, *J. Phys. Chem. B*, 2003, **107**, 597.

Table 1 Sizes of experimental cleaned QD samples (CdS-X (X=1-5)) determined by TB theory.

QDs	λ (nm)	excitation energy (eV)	diameter (Å)
CdS-1	360.13	3.42	16.12
CdS-2	369.23	3.36	17.22
CdS-3	379.88	3.26	19.23
CdS-4	381.66	3.25	19.78
CdS-5	386.10	3.21	20.70

Table 2 Geometrical parameters for passivated QDs.

property	model QDs		
	QD1	QD2	QD3
1.Bond length (Å)			
Cd(3)-S	2.49-2.56	2.50-2.82	2.47-2.68
Cd(4)-S	2.64-2.80	2.58-2.84	2.53-2.88
Cd_A-O_A	2.23-2.25	2.20-2.25	2.23-2.25
Cd_B-O_B	2.32	2.31-2.33	2.28(near H), 2.32
Cd_B-O_A	2.42-2.45	2.43-2.47	2.40-2.46
C-O_A	1.28	1.29	1.28
C-O_B	1.24	1.24	1.24
2.Bond angle (°)			
S-Cd(3)-S	128.70-140.28	98.60-138.68	116.18-143.99
S-Cd(3)-O	106.10-117.00	100.95-124.22	104.96-116.15
S-Cd(4)-S	108.54-110.73	99.07-128.18	103.95-116.12
Cd-S(3)-Cd	94.73-105.88	92.96-110.20	89.78-111.52
Cd-S(4)-Cd	109.21-109.76	102.09-115.80, (68.92-149.74†)	98.40-118.74
3.Angle between O-Cd-O and S-Cd-S plane (°)			
φ(Acetates)	88.52-90.79	62.05-102.407	87.94-92.371
φ'(Dye)	95.427	105.247	84.58

QD# presented in Fig. 2.
† Range for the surface 4-coordinated S atoms near 6 acetates for QD2.

Table 3 Optical data for theoretical absorption spectra in gas phase.

system	nstates, E*(eV)	excited states (@S_0)	excitation energy E(eV)	wavelength (nm)	oscillator strength	eigen value (NTO)
Dye	10, 5.64	$S_0 \rightarrow S_1$	3.39, *3.40[65],*3.32[66]	366.16	0.5407	
QD1	40, 4.15	$S_0 \rightarrow S_{11}$	3.28	378.48	0.1249	
		$S_0 \rightarrow S_{69}$	4.04	306.75	0.1327	
QD2	40, 3.33	$S_0 \rightarrow S_1$	2.66	466.29	0.0594	
		$S_0 \rightarrow S_5$	2.75	450.61	0.0585	
		$S_0 \rightarrow S_6$	2.75	450.56	0.0586	
QD3	40, 3.34	$S_0 \rightarrow S_{13}$	3.02	410.40	0.0814	
		$S_0 \rightarrow S_{22}$	3.15	393.63	0.0758	
Dye-QD1	10, 3.43	$S_0 \rightarrow S_3$	3.21	386.34	0.1830	0.8678
		$S_0 \rightarrow S_6$	3.30	375.74	0.5761	0.7658
		$S_0 \rightarrow S_9$	3.40	364.13	0.1013	0.9791
Dye-QD2	55, 3.37	$S_0 \rightarrow S_{41}$	3.28	377.42	0.2280	0.3909
		$S_0 \rightarrow S_{42}$	3.29	376.79	0.4893	0.4805
		$S_0 \rightarrow S_{43}$	3.30	376.14	0.1023	0.5231
Dye-QD3	55, 3.39	$S_0 \rightarrow S_{43}$	3.29	376.45	0.2551	0.8818
		$S_0 \rightarrow S_{45}$	3.32	373.79	0.3372	0.9270
		$S_0 \rightarrow S_{51}$	3.36	369.36	0.1625	0.9850

E* is the maximum energy obtained in each case by using the maximum number of states given, nstates. Also given for comparison are the theoretical values obtained from the literature(*).

Table 4 Optical data for theoretical absorption spectra with solvents effect using PCM model.

system	solvents	nstates, E*(eV)	excited states (@S_0)	excitation energy E(eV)	wavelength (nm)	oscillator strength	eigenvalue (NTO)
dye	chloroform	10, 5.73	$S_0 \rightarrow S_1$	3.16(2.76) **2.78[46,a]	392.50	0.7206	
	toluene	10, 5.69	$S_0 \rightarrow S_1$	3.19(2.81) **2.80[77,b]	388.67	0.7200	
dye-QD1	chloroform	10, 3.39	$S_0 \rightarrow S_1$	3.07	404.23	0.2352	0.9957
			$S_0 \rightarrow S_2$	3.14	394.97	0.2037	0.9496
			$S_0 \rightarrow S_3$	3.18	389.33	0.3441	0.8579
			$S_0 \rightarrow S_4$	3.20	387.15	0.5475	0.7878
			$S_0 \rightarrow S_5$	3.21	386.03	0.1406	0.9779
	toluene	10, 3.44	$S_0 \rightarrow S_2$	3.14	394.49	0.1891	0.9071
			$S_0 \rightarrow S_3$	3.17	391.26	0.4234	0.9071
			$S_0 \rightarrow S_4$	3.20	387.61	0.4164	0.7310
			$S_0 \rightarrow S_5$	3.21	386.12	0.4140	0.8640

E* is the maximum energy obtained in each case by using the maximum number of states given, nstates. Also given for comparison are the experimental values for this work in parentheses and experimental values obtained from the literature(** [a] in ethanol and [b] in methanol).

Table 5 Optical data for theoretical emission spectra.

system	solvents	excited states	excitation energy E(eV)	wavelength (nm)	oscillator strength	eigenvalue (NTO)
Dye	chloroform	$S_0 \leftarrow S_1(@S_1)$	2.90(2.59) **2.53[46,a]	426.67	0.7332	
	toluene	$S_0 \leftarrow S_1(@S_1)$	3.00(2.59) **2.64[77,b]	413.25	0.6263	
Dye-QD1	chloroform	$S_0 \leftarrow S_1(@S_1)$	2.72	456.22	0.0053	0.9997
		$S_0 \leftarrow S_2(@S_2)$	1.73	717.39	0.0004	0.9999
		$S_0 \leftarrow S_3(@S_3)$	3.08	402.32	0.4881	0.8886
	toluene	$S_0 \leftarrow S_2(@S_2)$	1.90	653.22	0.0144	0.9989
		$S_0 \leftarrow S_4(@S_4)$	3.07	403.85	0.4373	0.7489

Also given for comparison are the experimental values for this work in parentheses and experimental values obtained from the literature(** [a] in ethanol and [b] in methanol).

Table 6 Theoretical open-circuit voltage for dye-sensitized QDs.

system	HOMO(eV) (on dye)	LUMO(eV) (on QD)	V_{OC}(V)
dye-QD1	-5.63	-2.72	2.91
dye-QD2	-5.76	-3.18	2.58
dye-QD3	-5.55	-3.21	2.34

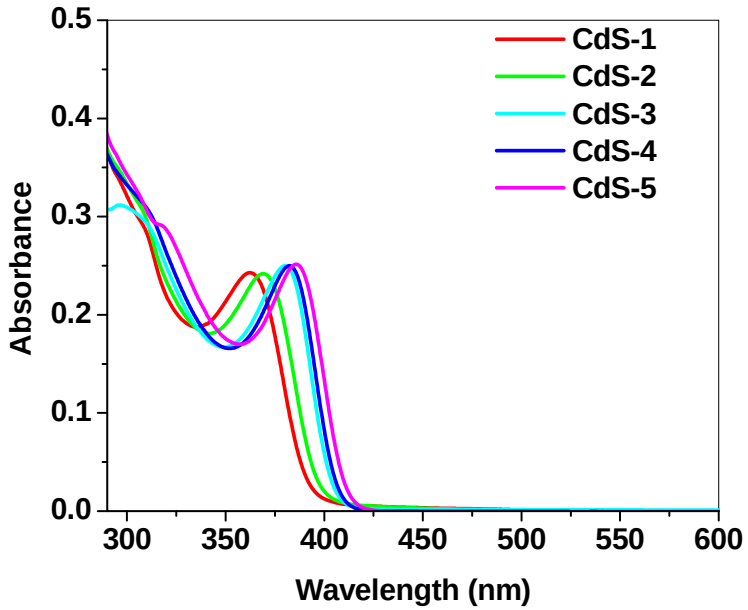

Fig. 1 Experimental optical absorption spectra of cleaned QDs, CdS-X (X=1-5).

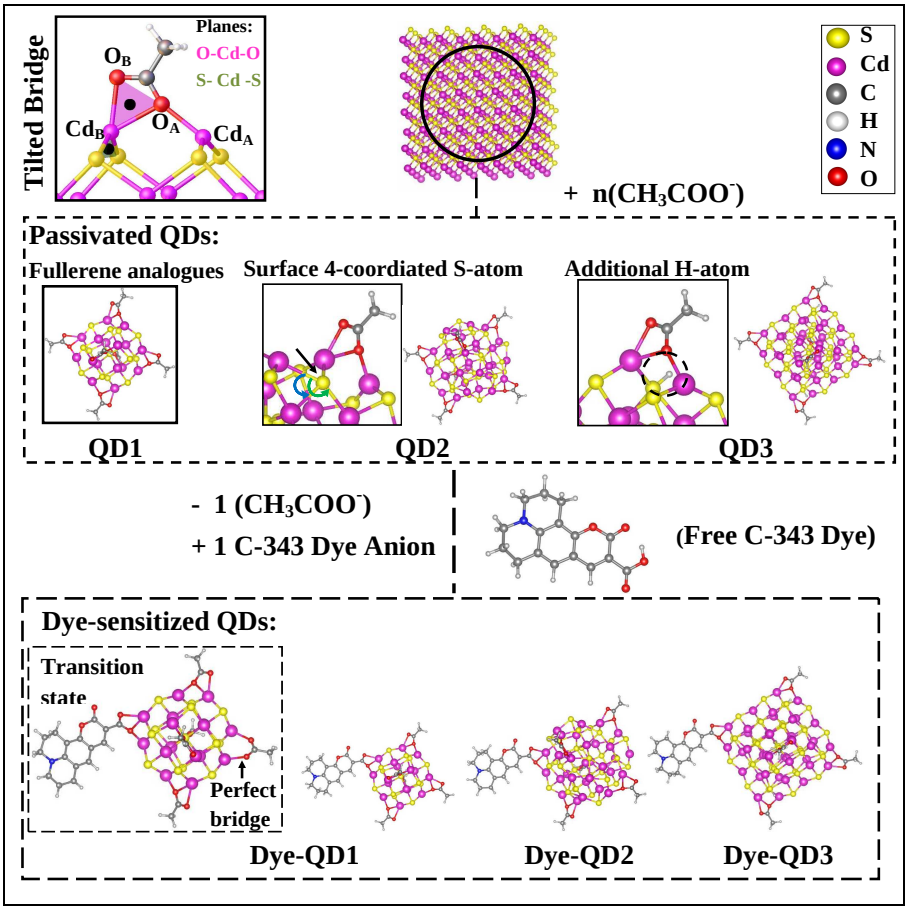

Fig. 2 Optimised structures of passivated and dye-sensitized QDs in vaccum. The procedure for constructing the quantum dots is presented. The notation of the QDs (QD#) refers to the cluster size presented in the text. Green and blue curved arrows in QD2 are the bond angles 149.74° and 68.92 °respectively.

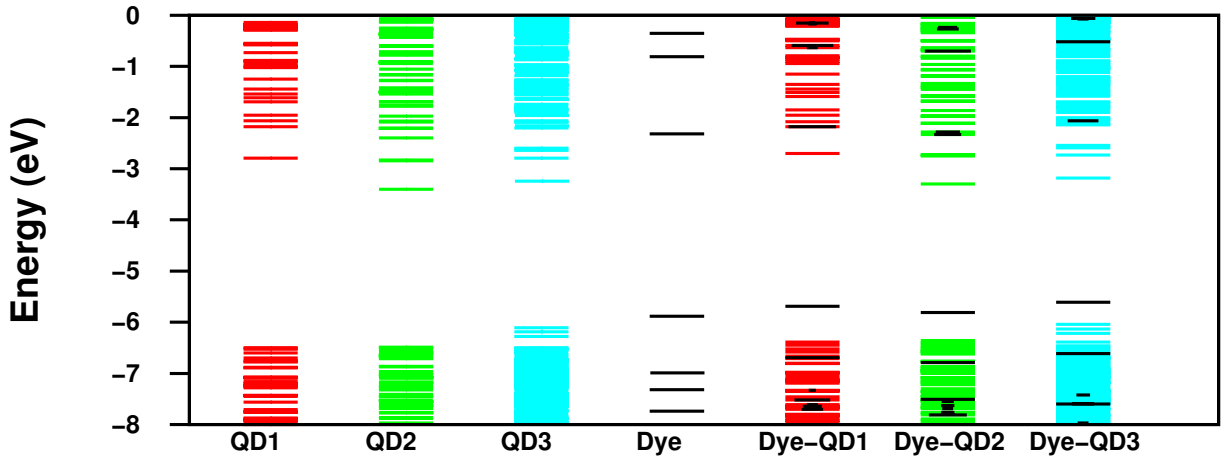

Fig. 3 Energy levels for the model passivated and dye sensitized QDs. The black lines in the dye-QD system refer to the levels arising from the dye and their width refers to the percentage contribution of the dye.

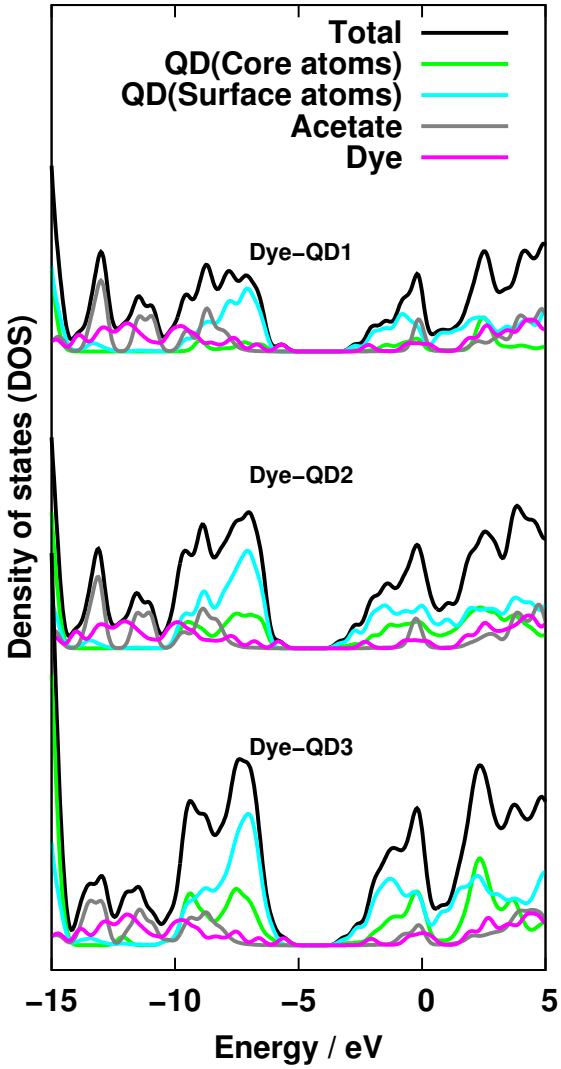

Fig. 4 Projected density of states for dye-sensitized QDs with half width of 0.5 eV.

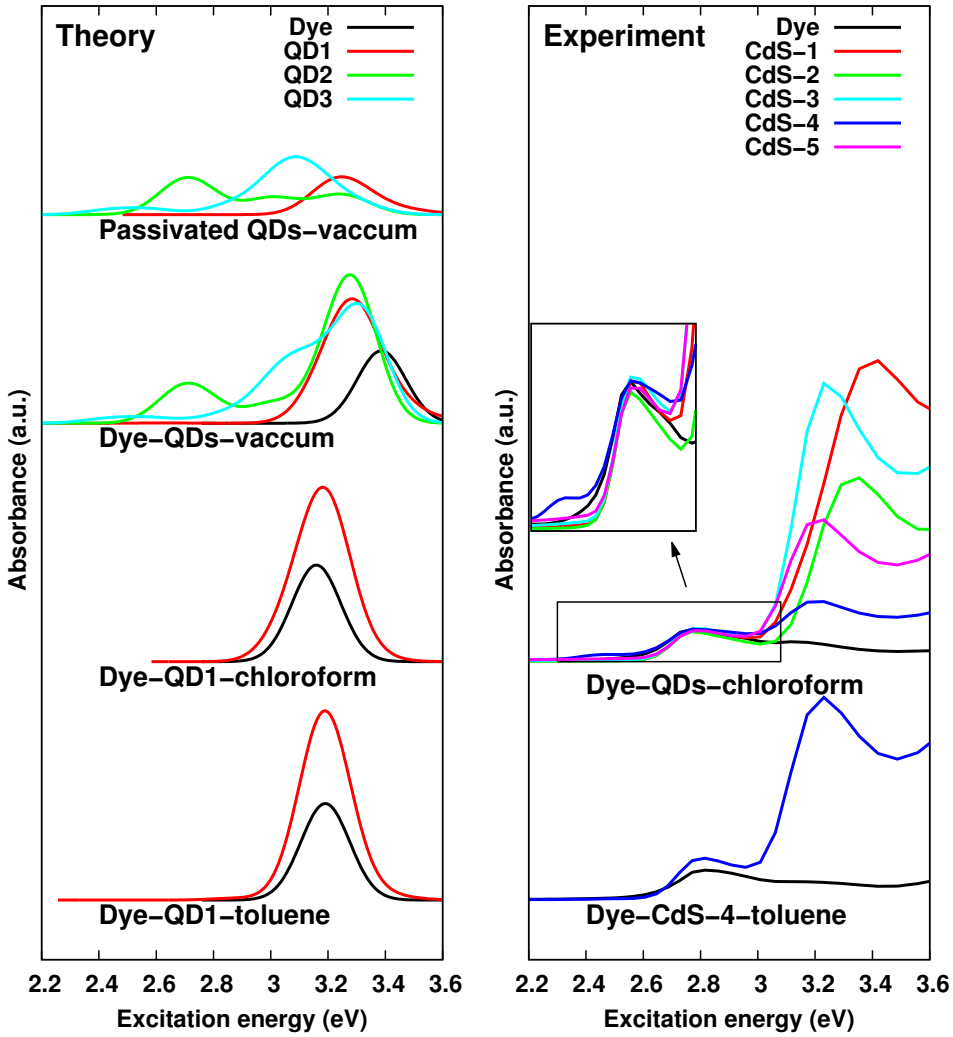

Fig. 5 Optical absorption spectra of C-343 dye-sensitized QDs.

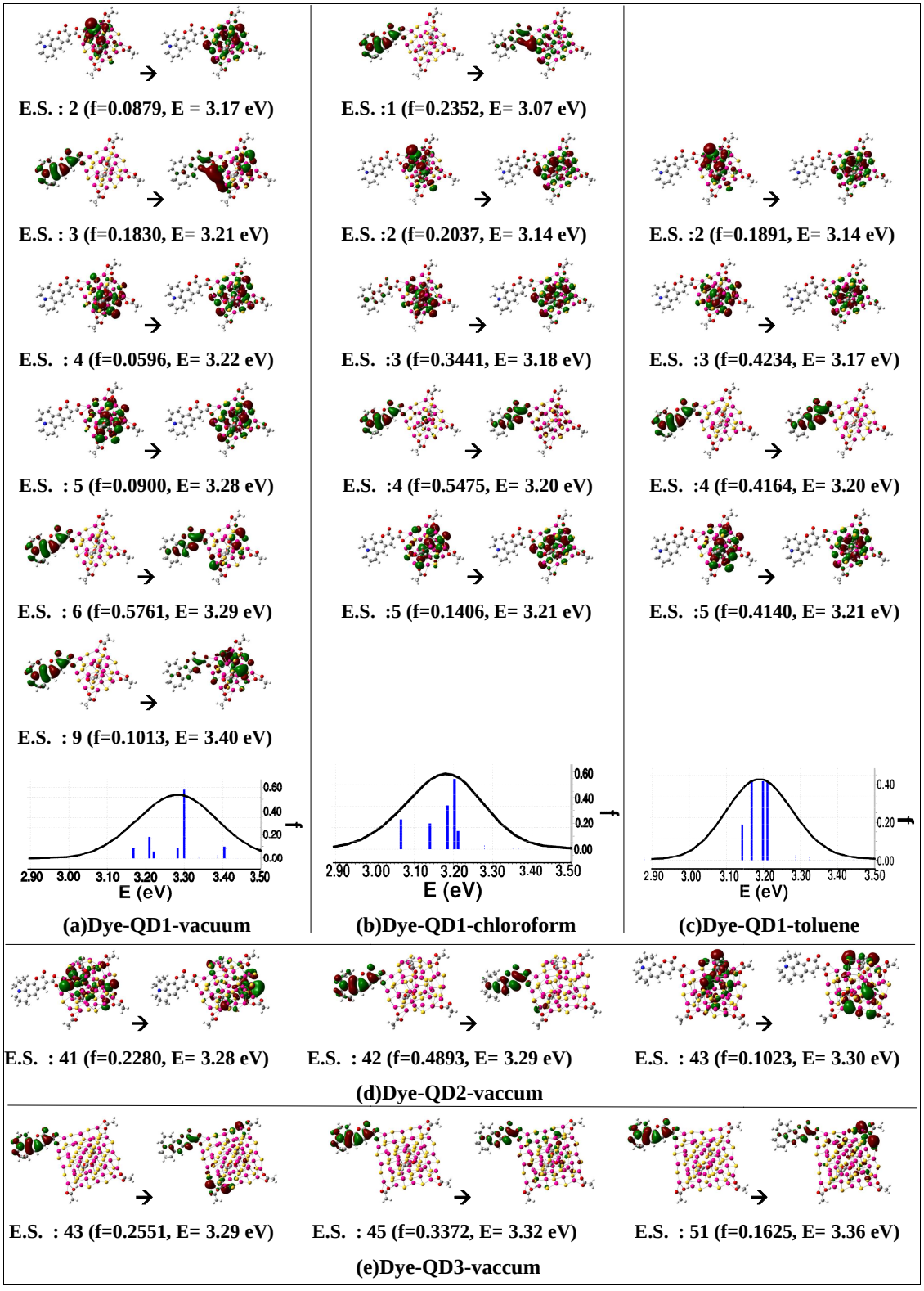

Fig. 6 Natural transition orbitals (charge transfer during absorption).

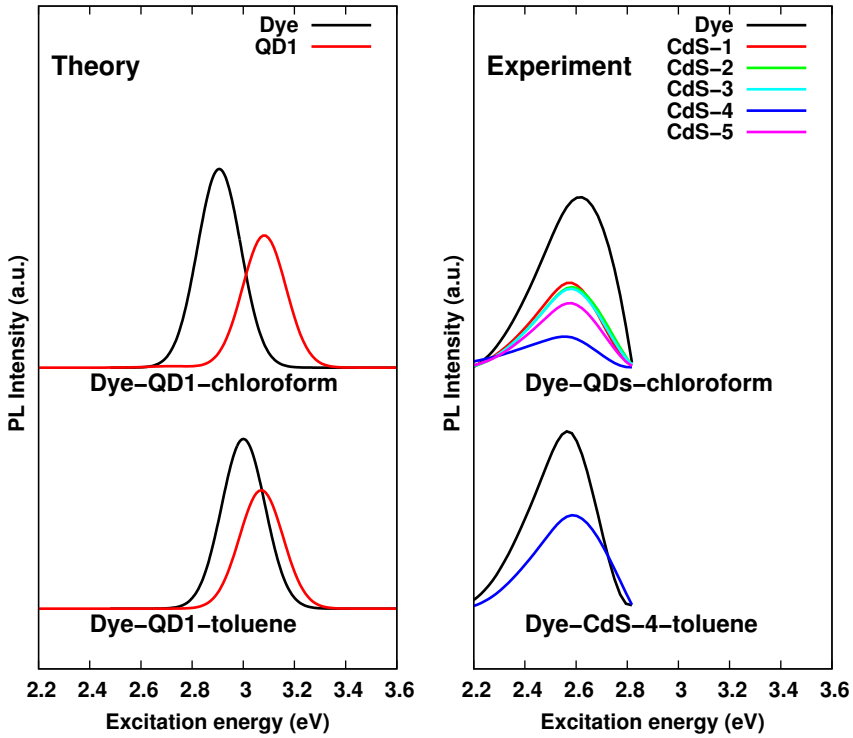

Fig. 7 Optical emission spectra of C-343 dye-sensitized QDs.

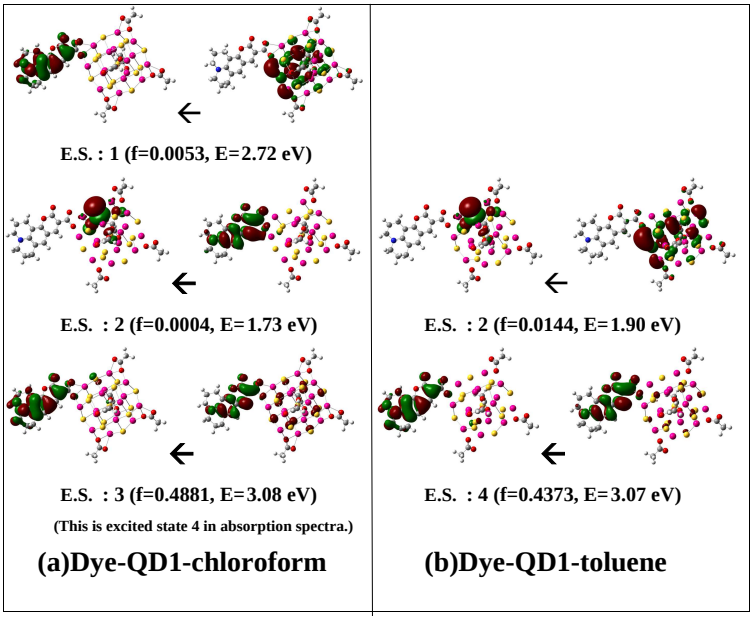

Fig. 8 Natural transition orbitals (charge transfer during emission).